VARIFORC processing examples

First-point correction

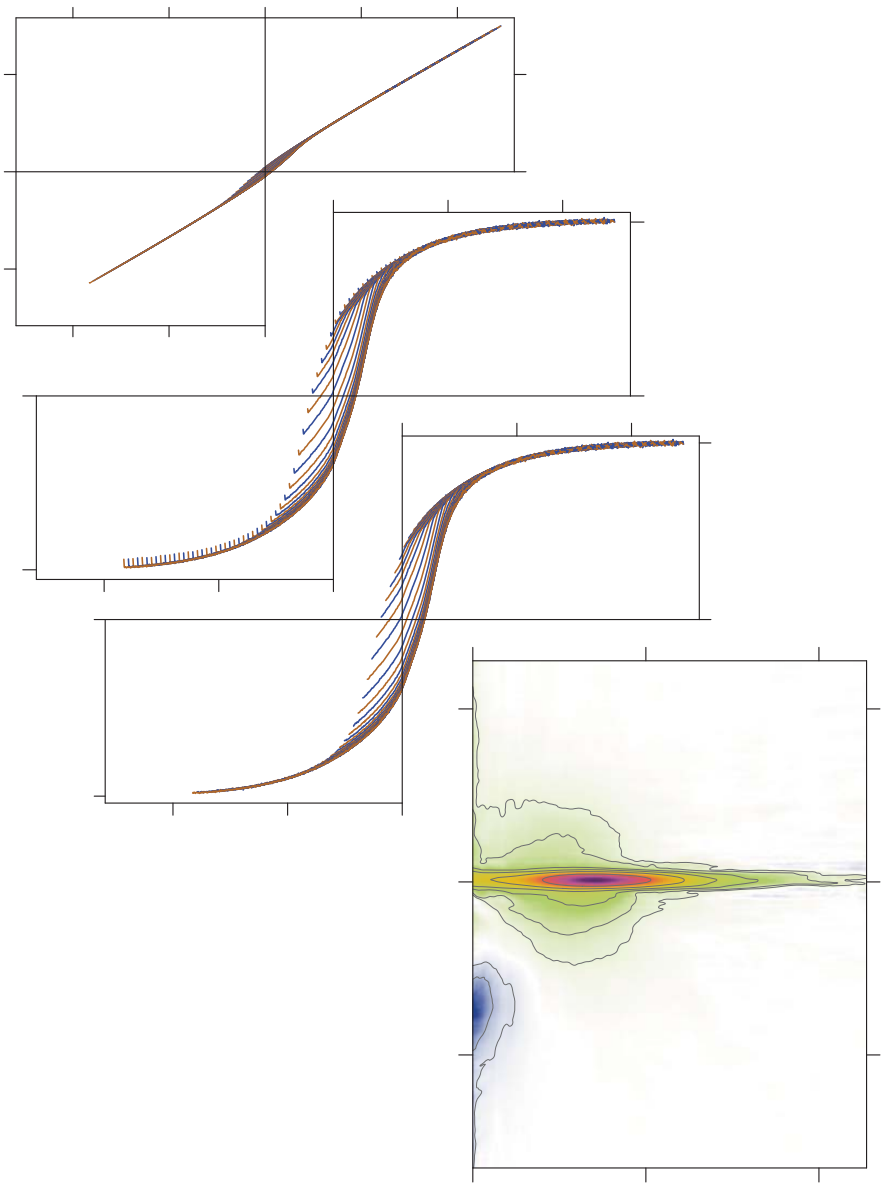

About this example

The measured material comes from the outer rim of a ferromanganese crust retrieved from the top of a deep-sea hill at 4830 m water depth in the Central Pacific [*Friedrich and Wiechowski*, 1980]. The outer rim of consists of compact layers of black amorphous ferromanganese oxyhydroxides with 17-26% total Fe content. FORC measurements of this sample are challenging because of the very small concentration of magnetic minerals and the overwhelming paramagnetic contribution from the amorphous phases. This means that the magnetometer was operated at a relatively low sensitivity to accommodate the full-scale paramagnetic contribution, resulting in a lowered signal-to-noise ratio for the ferrimagnetic signal. This is probably also the reason for particularly evident artifacts affecting the first measurement point of each curve. Because these artifacts create a vertical ridge in the FORC diagram, which is similar to the signature of magnetic viscosity [*Pike et al.*, 2001], this example has been selected in order to illustrate how anomalous first-point measurements can be recognized and corrected.

FORC measurements

- Measuring instrument: PMC MicroMag 3900 VSM.
- Specimen: ~3 mm fragment
- Preparation: Cemented to the sample holder.
- FORC measurement protocol:

```
Hc1 = 0      , Hc2 = 0.15 T
Hb1 = -0.03 T, Hb2 = +0.09 T
Hsat = 0.3 T
Averaging time       = 0.1 s
Pause at calibration = 0.2 s
Pause at reversals   = 0.5 s
Pause at saturation  = 0.2 s
Smoothing = 5 (adds a 5-point margin to the measured range)
```

- Derived measurement parameters:

```
Number of curves: 553
Calibration measurements at 0.246 T
Mean size of field steps = 0.5 mT (maximum resolution of the FORC diagram)
```

- **Notes on measurements.** Measurements are close the sensitivity limit of the instrument, with a magnetic moment of 5 μAm^2 at 0.2 T and, most importantly, a saturation remanent moment of only 0.2 μAm^2 (the nominal RMS noise with 0.1 s averaging time is <0.01 μAm^2). Therefore, the same set of FORC measurements has been repeated 16 times and averaged with VARIFORC in order to increase the signal-to-noise ratio.

About VARIFORC processing options used in this example

VARIFORC modules are controlled by processing options stored in so-called parameter files. Parameter files used to process FORC data related to this example can be find in the folder containing this document. These are:

1. Import and correct FORC measurements (`ImportFORC` module):

- `FMK1_VARIFORC_ImportFORC_parameters.txt`: no first-point correction
- `FMK1-fpc_VARIFORC_ImportFORC_parameters.txt`: first-point correction

2. Calculate the FORC diagram (`CalculateFORC` module):

- `FMK1-SF5_VARIFORC_CalculateFORC_parameters.txt`: conventional processing with a constant smoothing factor (SF = 5).
- `FMK1-vari_VARIFORC_CalculateFORC_parameters.txt`: optimized processing with variable smoothing.

3. Isolate the central ridge (`IsolateCR` module):

- `FMK1-Automatic_VARIFORC_IsolateCR_parameters.txt`: automatic initial range selection.
- `FMK1-Manual_VARIFORC_IsolateCR_parameters.txt`: manually optimized initial range selection.

Single suite of FORC measurements

A single set of FORC measurements obtained with the PMC MicroMag 3900 VSM is shown in Plate 1, which is based on graphical outputs from **`ImportFORC`**. These measurements can be considered as a good example for the instrument capabilities. The maximum separation between consecutive curves is 10 nAm^2, and the total magnetization of the dominant FORC signature of this sample, i.e. the so-called central ridge, corresponds to 100 nAm^2. These magnetic moments are generated by as few as 0.2 and 2 μg of single-domain magnetite (Fe_3O_4) particles, respectively. On the other hand, the standard deviation of the 0.5 mT measurement field steps does not exceed 0.03 mT. The typical magnetic moment change over a single field step is only 2.5 nAm^2, and is equivalent to the effect produced by switching ~350 magnetite single-domain crystals.

Due to relatively strong paramagnetic contributions, the measurement range had to be set to ±5 μAm^2, although the saturation magnetization of ferrimagnetic contributions is ~10 times smaller, thereby loosing precious measurement precision. This might be the reason for unusually evident anomalies in first-point measurements (Plate 1b-c), which fall systematically above the curve trends. The maximum amplitude of these anomalies is 30 nAm^2, i.e. only ~4 times the measurement noise RMS, and therefore barely noticeable with stronger samples (see the VARIFORC processing example on rectangular hysteresis loops).

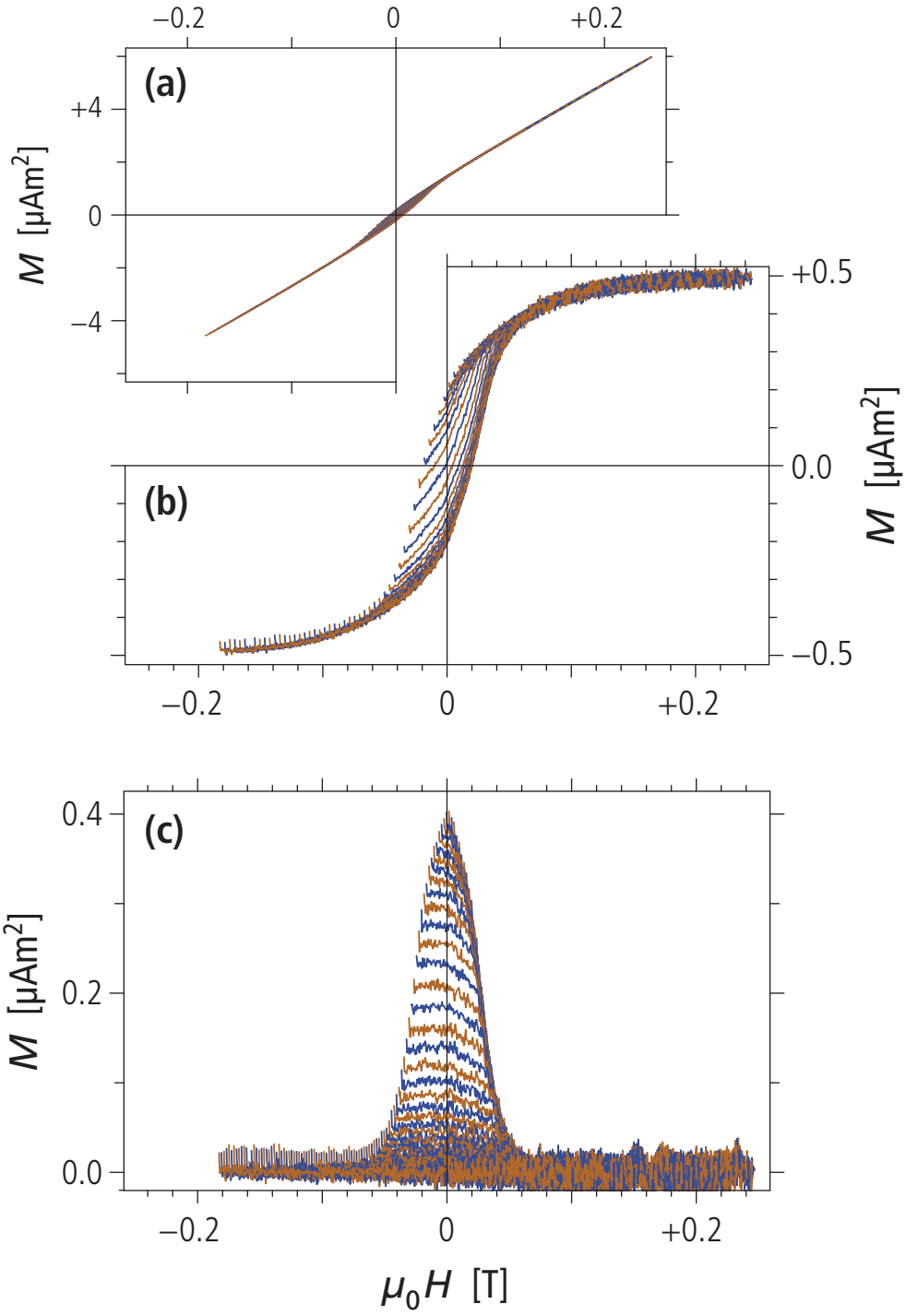

Plate 1. Single set of FORC measurements. Plots were generated by **`ImportFORC`** with minor editing. **(a)** Drift- and outlier-corrected measurements. Every 8th curve (see `INPUT 14` of the parameter file) is shown for clarity. **(b)** Same as (a), after paramagnetic correction with an approach-to-saturation model based on measurements at field amplitudes ≥0.13 T. **(c)** Same as (b), after subtraction of the lower hysteresis branch reconstructed from the FORC measurements (see `INPUT 21` of the parameter file). Every 4th curve is shown for clarity.

Multiple measurements average without first-point correction

Sixteen sets of identical measurements have been imported and averaged in a single **ImportFORC** run (see parameter file `FMK1_VARIFORC_ImportFORC_parameters.txt`). Each set has been corrected individually for drift and outliers. A weighted average of the corrected sets has been calculated by weighting each set according to the estimated level of measurement noise, so that worse sets count less than better ones. This procedure minimizes measurement error contributions to the average and is part of the standard processing algorithm of **ImportFORC**. In this example, weights ranged from 0.4 (worse set) to 1.5 (best set).

Measurements are dominated by a strong paramagnetic contribution (Plate 1a), which, at full range, is ~25 times stronger than the saturation remanence. Accordingly, details of the ferrimagnetic hysteresis are barely recognizable. A paramagnetic correction has been applied with **ImportFORC** using the approach-to-saturation law $M = M_s - cH^{-\beta} + \chi_{hf} H$, where M is the magnetization measured over the saturation range (i.e., where the hysteresis loop is completely close), M_s is the saturation magnetization, H is the applied field, χ_{hf} is the high-field susceptibility, β is the approach-to saturation exponent, and c is a constant [*Fabian*, 2006]. In this example, the saturation range was identified with measurements in field amplitudes $|H| > 0.13$ T (see `INPUT 18` in the parameter file), and, for better model stability, $\beta = 2$ was set in accordance with the single-domain nature of the ferrimagnetic hysteresis (see `INPUT 20` in the parameter file). Details of the ferrimagnetic hysteresis become evident after paramagnetic correction, along with residual measurement noise, and, most importantly, anomalous first-point measurements lying above the trend of each curve.

First-point anomalies become more evident when the lower branch of the hysteresis loop reconstructed from FORC measurements is subtracted from each curve (Plate 1c). In this case, one can clearly see that first-point anomalies are highest at most negative fields (+30 nAm^2) and decrease uniformly to <10 nAm^2 in positive fields. For comparison, the standard deviation of measurement noise is ~6 nAm^2. The monotonic dependence of first-point anomaly amplitudes on H, along with the fact that only the first point of each curve is affected, excludes magnetic viscosity as a possible source, because viscosity effects (1) cannot occur in the saturated range of hysteresis and (2) usually extend over at least the first two measurement points of each curve.

First-point anomalies are often seen in FORC measurements of weak samples, as reported in other VARIFORC examples. Sometimes they overlap with a true magnetic viscosity signature (see VARIFORC example on volcanic ash). First-point artifacts can be eliminated with **ImportFORC**, as explained in the following.

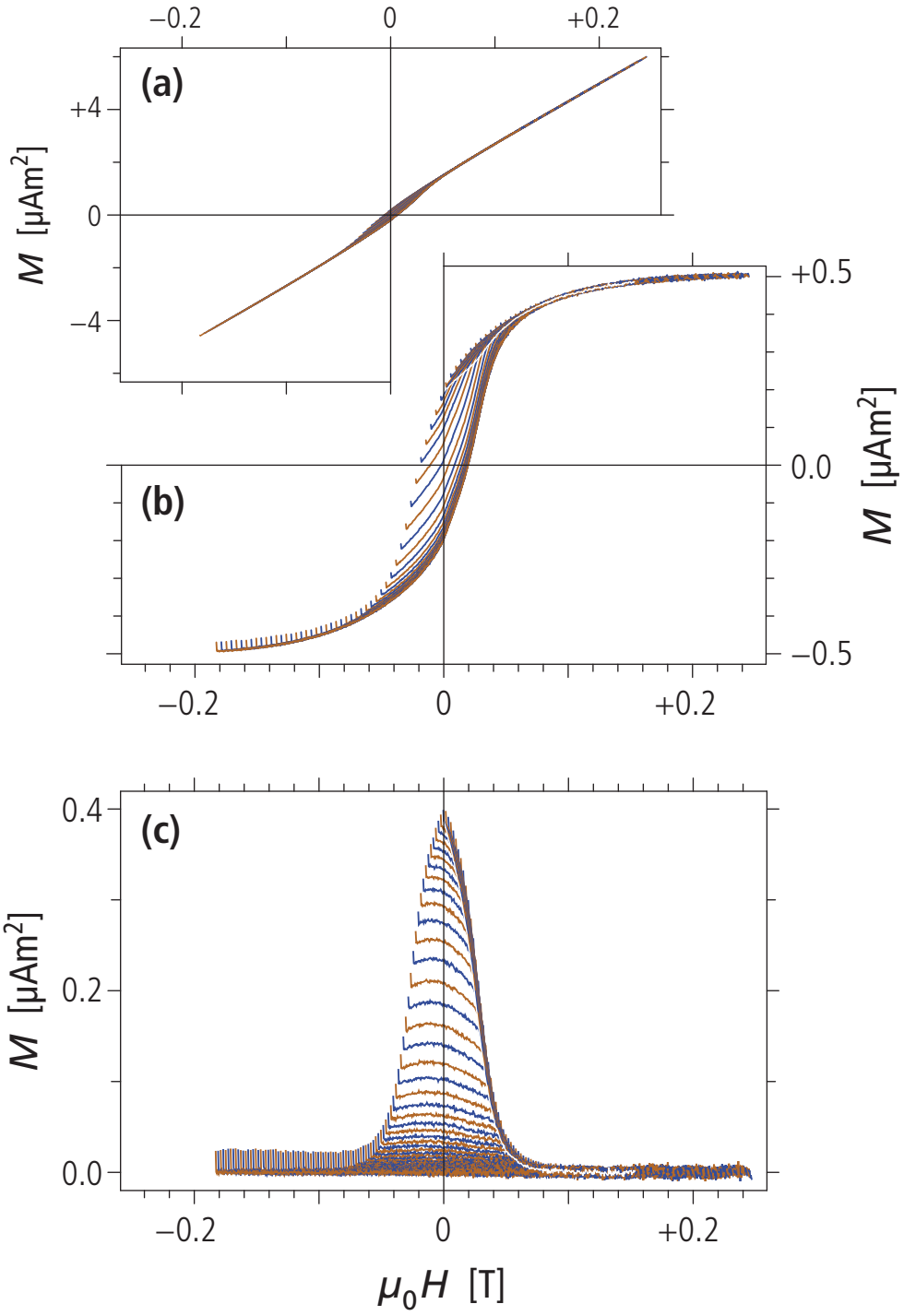

Plate 2. Averaged FORC measurements. Plots were generated by **ImportFORC** with minor editing. **(a)** Weighted average of the 16 measurement sets after drift and outlier correction. Every 8th curve (see INPUT 14 of the parameter file) is shown for clarity. **(b)** Same as (a), after paramagnetic correction with an approach-to-saturation model based on measurements at field amplitudes ≥0.13 T. The ideal central ridge locus, corresponding to $H = -H_r$, is highlighted by a white line. Sharp slope discontinuities of the measured curves occur just above this line. **(c)** Same as (b), after subtraction of the lower hysteresis branch reconstructed from the FORC measurements (see INPUT 21 of the parameter file). Every 4th curve is shown for clarity. The ideal central ridge locus is highlighted by a white line.

Multiple measurement average with first-point correction

First-point artifacts can be eliminated with **ImportFORC** using the INPUT 08 option in the parameter file (see FMK1-fpc_VARIFORC_ImportFORC_parameters.txt). This options offers the possibility to correct first-point artifacts by changing the amplitude of the first field step (to be used with some earliest versions of the FORC measurement protocol and no longer required), or by replacing the magnetic moment measurement with a value obtained from second-order polynomial extrapolation of the curve trend set by adjacent points. The number of points taken into consideration for this extrapolation depends on the smoothing factor chosen for error estimation purposes (INPUT 10), which is usually comprised between 2 and 5. Smaller smoothing factors are used to process data containing high-resolution features, while higher smoothing factors are better suited to smooth measurement curves (see Chapter 3 of the VARIFORC user manual). Ideally, extrapolation is performed over a number of points that can be fitted with a second-order polynomial without introducing additional errors. Second-order polynomials can fit magnetic viscosity effects at the beginning of each curve [*Pike et al.*, 2001], so that true viscosity signatures – which always extend over several points – are not removed by the extrapolation procedure.

Processed FORC data with first-point correction are shown in Plate 3. First-point corrected measurements collapse onto a single curve over the saturation range of hysteresis, unlike the case of uncorrected measurements (Plate 2). A general increase of the measurement noise level towards positive fields is now clearly recognizable.

Overall, the typical signature of non-interacting single-domain magnetic particles can be recognized in these measurements (see the VARIFORC example on magnetofossil-bearing sediments). In particular, the so-called central ridge signature [*Egli et al.*, 2010] is recognizable from the sharp slope changes above the white line, which marks the position on each curve where $H = -H_r$ (Plate 3b,c).

The envelope of all curves in Plate 3c coincides with the even component of the hysteresis loop, i.e. the difference between upper and lower branches [*Fabian and Dobeneck*, 1997]. Unlike the magnetofossil-bearing sediments, where the curve envelope is a Gaussian-like function, a cusp occurs at $H = 0$. This cusp originates from particles with a nearly vanishing coercivity (see the VARIFORC example on dispersed magnetosomes).

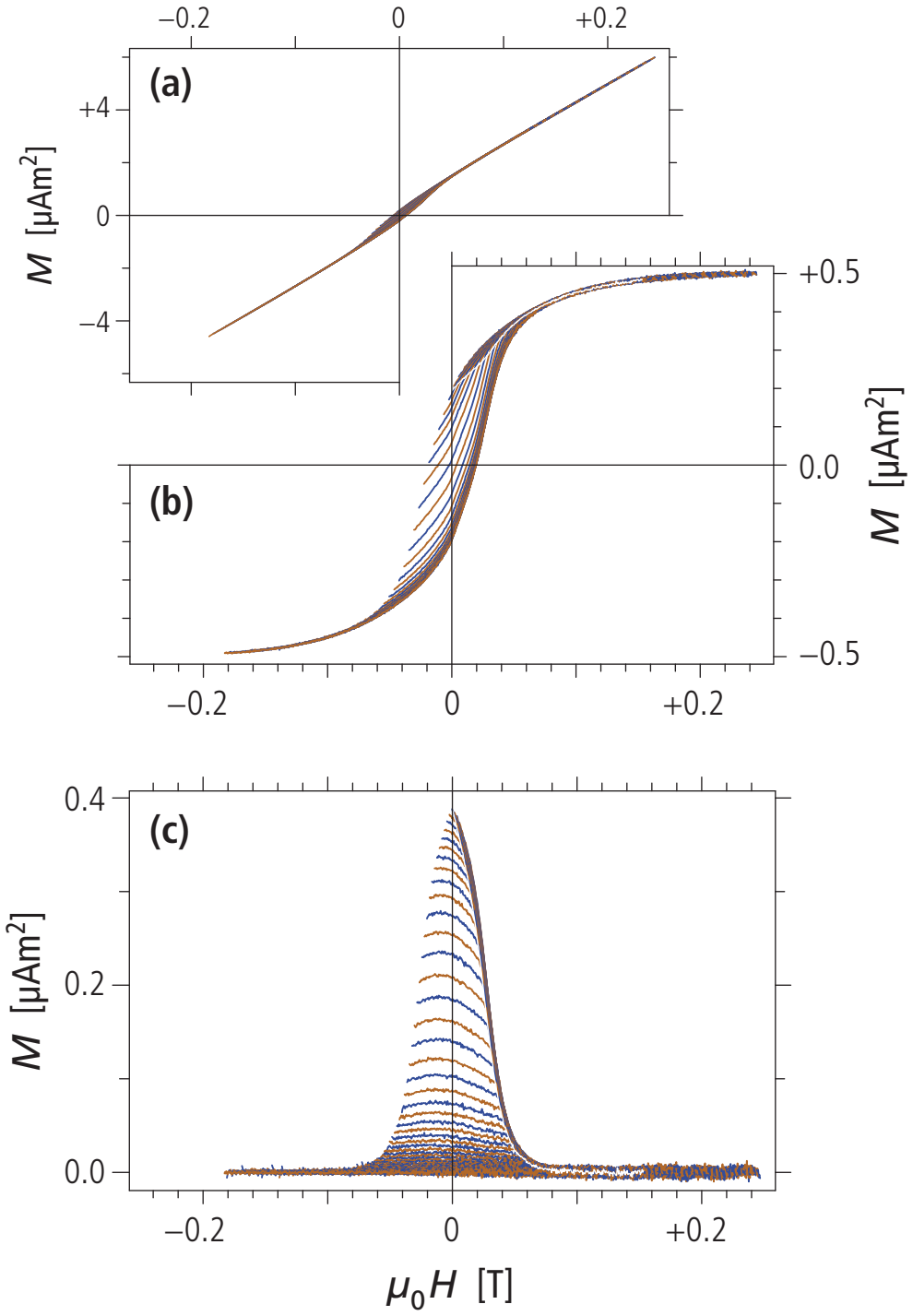

Plate 3. Averaged FORC measurements with first-point correction. Plots were generated by **ImportFORC** with minor editing. **(a)** Weighted average of the 16 measurement sets after drift, outlier, and first-point corrections. Every 8th curve (see INPUT 14 of the parameter file) is shown for clarity. **(b)** Same as (a), after paramagnetic correction with an approach-to-saturation model based on measurements at field amplitudes ≥0.13 T. The ideal central ridge locus, corresponding to $H = -H_r$, is highlighted by a white line. Sharp slope discontinuities of the measured curves occur just above this line. **(c)** Same as (b), after subtraction of the lower hysteresis branch reconstructed from the FORC measurements (see INPUT 21 of

the parameter file). Every 4th curve is shown for clarity. The ideal central ridge locus is highlighted by a white line.

Hysteresis parameters (M_{rs}/M_s = 0.38 and H_{cr}/H_c = 1.47) plot on the theoretical mixing line between single-domain and multidomain particles in the Day diagram (Plate 4): however, as shown later in this example, this interpretation is contradicted by the FORC diagram, whose signatures suggest a mixture of non-interacting and interacting single-domain particles typical for magneto-fossils. In fact, hysteresis parameters are compatible with the empirical trend defined by magneto-somes extracted from cultured magnetotactic bacteria (green dots, *Li et al.* [2012]).

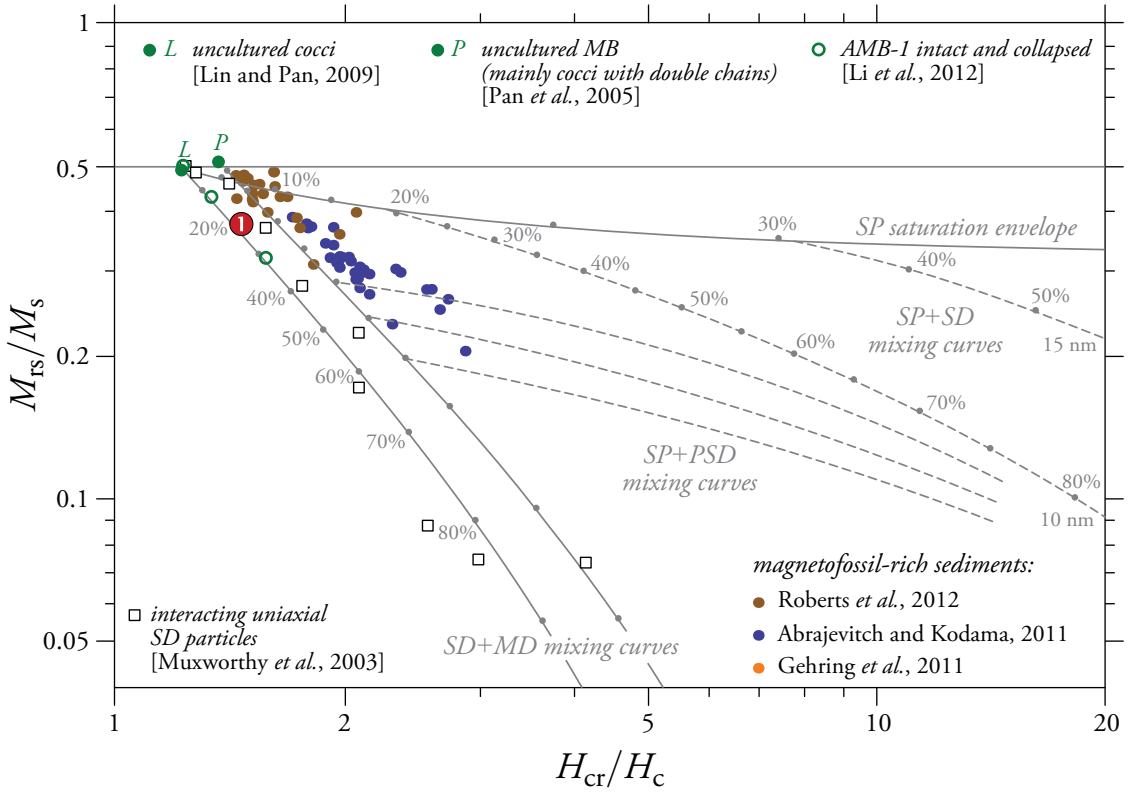

Plate 4. Hysteresis parameters in the Day diagram. Day diagram after *Dunlop* [2002], showing hysteresis properties of magnetofossil-bearing sediments and magnetotactic bacteria samples (dots). Theoretical mixing trends are shown in gray. The ferromanganese crust of this example is marked with ❶.

First-point artifacts and the vertical ridge

First measurement points that are systematically offset produce a vertical ridge along $H_c = 0$ in the FORC diagram (Plate 5a). The interpretation of this ridge generated some confusion in the past. A known physical origin for a vertical ridge at $H_c = 0$ is magnetic viscosity [*Pike et al.*, 2001]: as the field sweep is reversed at the beginning of each curve, irreversible magnetization losses continue to occur, triggered by thermal activations, even with applied fields that increase in time. An essential condition for thermally activated processes to occur is that the magnetic system is in an intermediate state that does not coincide with positive and negative saturation: once saturation is reached, there are no magnetic transitions that can be thermally activated. Therefore, the maximum vertical extension of the central ridge is limited by $\pm H_s$, where H_s is the field amplitude above which the major hysteresis is fully closed. A typical example is shown in Figure 5 of *Pike et al.* [2001].

In order to represent reversible magnetization processes that are not captured by the FORC measurement protocol, *Pike* [2003] proposed a FORC processing procedure that introduces a vertical, so called "reversible ridge" along $H_c = 0$, which accounts for reversible processes, ensuring that the integral of the FORC diagram over H_c and H_b yields the saturation magnetization M_s. The large ridge amplitude, and its "leaking" into the FORC space at low measurement resolution, led to the misconception that the left limit of FORC space is unstable and does not convey useful information. For this reason, modern FORC processing software does not add a "reversible ridge" to the data. Furthermore, algorithms that do not create artifacts along $H_c = 0$ are used [*Winkhofer and Zimanyi*, 2006; *Harrison and Feinberg*, 2008; *Egli*, 2013].

In our example, the vertical ridge calculated from data with uncorrected first-point measurements (Plate 5a) extends well beyond the range where the hysteresis loop is open (i.e. ±0.1 T), with monotonically decreasing amplitudes from negative to positive values of H_b. On the other hand, the vertical ridge is almost completely absent in the FORC diagram calculated from first-point-corrected data (Plate 5b). Residual amplitudes along $H_c = 0$ appear to be correlated with H_b (i.e., negative over the lower quadrant and positive over the upper quadrant) and might represent small artifacts affecting the second measurement point of each curve.

A possible matter of concern with first-point correction is that they might remove – wholly or in part – the signature of magnetic viscosity. Such signature, however, is an exponentially decaying process in the time domain, therefore extending beyond the first measurement in each curve. In this case, extrapolation of the trend set by the measuring points following the first one captures all magnetic viscosity effects with time constants larger than the time required to take the first measurement. A true viscosity signature revealed after removing first-point artifacts is discussed with the VARIFORC example based on a volcanic ash sample.

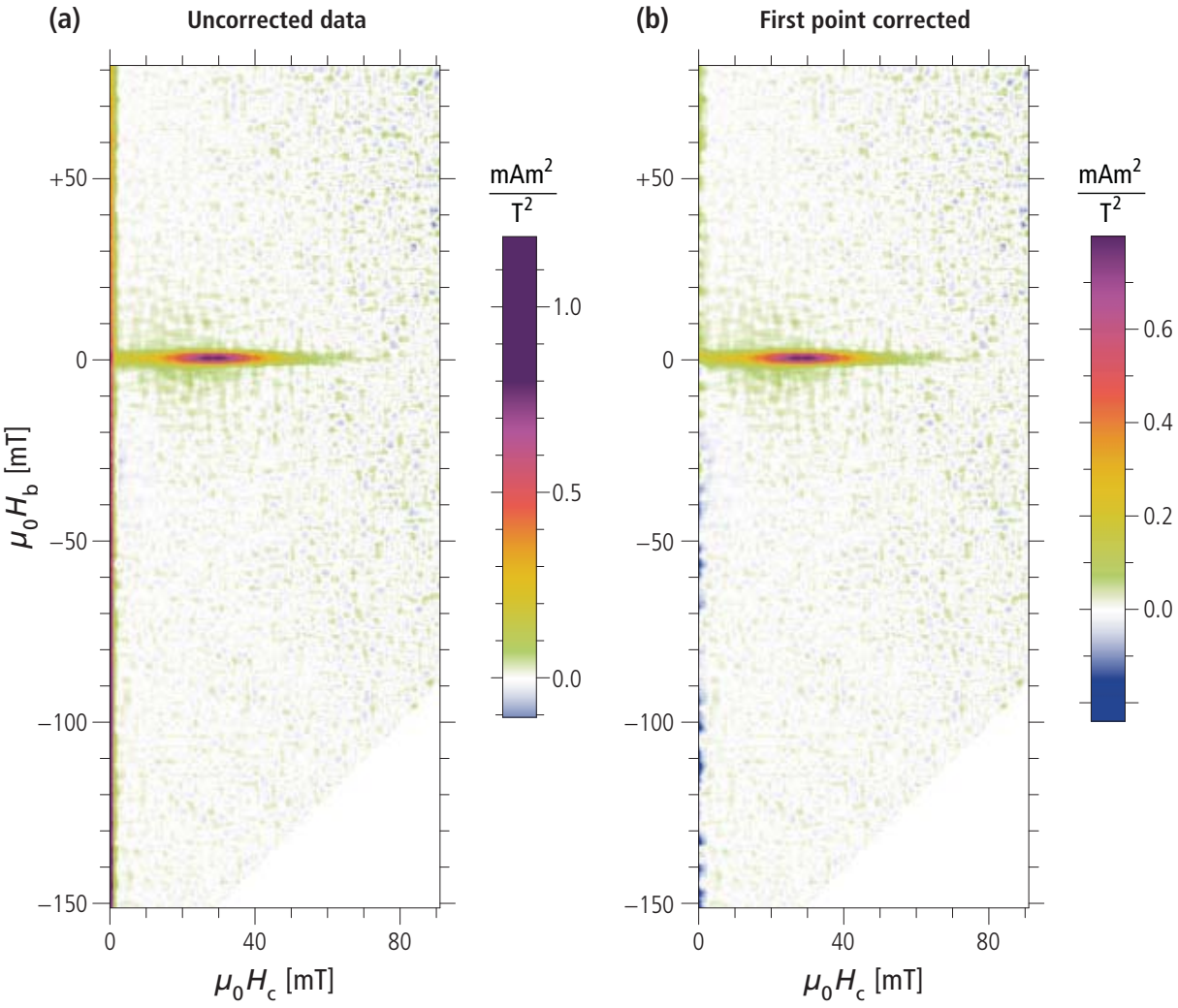

Plate 5. First-point artifacts in FORC diagrams and their correction. (a) FORC diagram calculated from uncorrected data (Plate 2). A vertical ridge along $H_c = 0$ extends over the whole range of measurements, with maximum amplitudes at most negative values of H_b. **(b)** FORC diagram calculated from first-point-corrected data (Plate 2). The vertical ridge is almost completely suppressed, with residual amplitudes at $H_c = 0$ being dominated by measurement noise. A residual correlation of these amplitudes with H_b might represent small artifacts affecting the second measurement point of each curve. Both FORC diagrams have been calculated with a constant smoothing factor SF = 5, and plotted with the same color scale for comparison purposes.

Complete VARIFORC analysis

FORC data processing with VARIFORC yields coercivity distributions and corresponding magnetizations derived from FORC measurement subsets. This additional information is important for establishing a link between FORC and conventional rock-magnetic parameters. As explained in the FORC tutorial provided with Chapter 8 of the VARIFORC user manual, three types of magnetization can be considered for this purpose: (1) the saturation remanence, M_{rs}, and the related coercivity distribution, f_{bk}, derived from backfield demagnetization data, (2) the irreversible component of the hysteresis loop, whose derivative with respect to the applied field defines a "coercivity distribution", f_{ir}, over positive and negative fields, with total magnetization M_{ir}, and (3) the coercivity distribution, f_{cr}, derived from the central ridge, with total magnetization M_{cr}.

In cases of FORC diagrams containing a central ridge, as in this example, quantitative analyses require proper ridge separation (Plate 6a-c). This operation is performed with **`IsolateCR`** exploiting the negligible intrinsic vertical extension of the central ridge, so that other FORC contributions can be linearly extrapolated under the area occupied by the ridge. If FORC measurements have been performed with high resolution (i.e., field steps ≤ 1 mT), and the central ridge is a dominant feature, as in this example, central ridge separation is a relatively uncritical operation that can be fully automatized (see parameter file `FMK1-Automatic_VARIFORC_IsolateCR_parameters.txt`). Automatic options can be further optimized by inspecting vertical profiles across the central ridge (see parameter file `FMK1-Manual_VARIFORC_IsolateCR_parameters.txt`), as explained in Chapter 6 of the VARIFORC user manual.

The FORC diagram (Plate 6a) closely resembles diagrams of partially collapsed magnetosome chains extracted from cultured magnetotactic bacteria [*Li et al.*, 2012]. The FORC diagram remaining after subtraction of the central ridge (Plate 6b) features the typical signature of magnetic moment rotation in single-domain particles, which has been described by *Newell* [2005]. This signature consists of equal negative and positive amplitudes over the lower quadrant, which are symmetric about the $H_b = -H_c$ diagonal. On the other hand, positive contributions over the upper quadrant in Plate 6b, which represent ~38% of the total FORC magnetization, bear the typical signature of strong magnetostatic interactions, which is manifested by oval contour lines around a central maximum [*Pike et al.*, 1999]. Overall, FORC diagrams in Plate 6a-c clearly indicate that this sample contains a mixture of non-interacting and strongly interacting single-domain particles, possibly corresponding to intact and collapsed magnetosome chains.

Additional information is gathered by the coercivity distributions derived from FORC measurements (Plate 6d), which appear to result from the combination of two magnetic components peaking at 0 and ~26 mT respectively. The second component is unusually narrow and resembles component "BS" in *Egli* [2004], which has been associated with magnetofossils. Both components contribute also to the central ridge. Integrals of the coercivity distributions shown in Plate 6d yield the total magnetizations listed in Plate 6e. All results shown in Plate 6 have been obtained directly with VARIFORC without additional calculations.

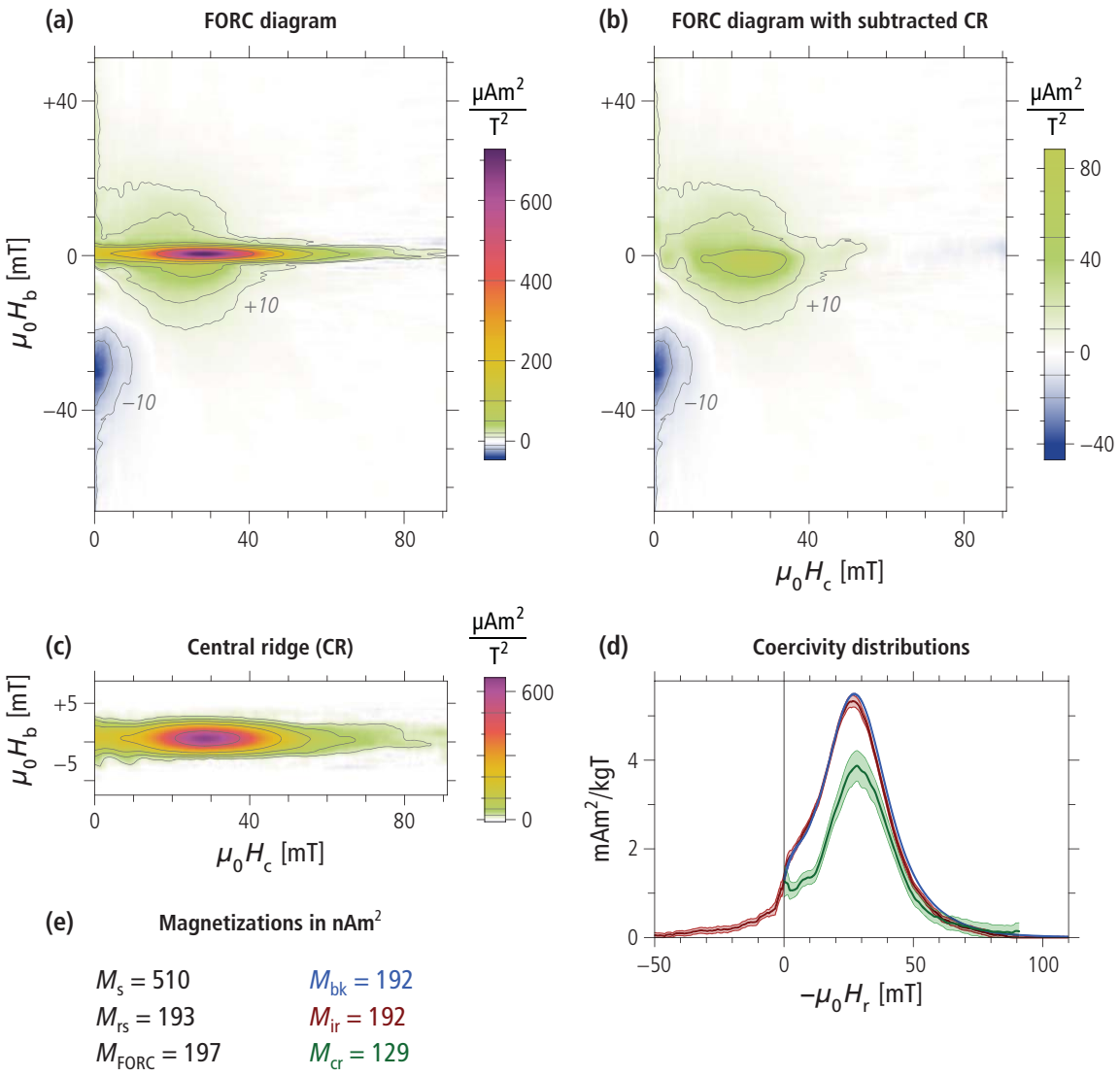

Plate 6. Complete VARIFORC analysis of a ferromanganese crust. (a) FORC diagram obtained with **`CalculateFORC`** (contour lines have been added with **`PlotFORC`**). Notice that the smallest contour level corresponds to 1.4% of the maximum FORC amplitude and is still fully significant. **(b)** FORC diagram remaining after subtraction of the central ridge with **`IsolateCR`**. The isolated central ridge is shown in **(c)** with a 2× vertical exaggeration, which highlights a small upward shift of the whole ridge. The shift is due to thermal activation effects and is a common feature for all sedimentary materials featuring a central ridge. All FORC diagrams share the same color scale. **(d)** Three types of coercivity distribution derived from FORC measurements, with shaded bands around each curve representing 2σ confidence levels. The first two distributions, f_{bk} and f_{ir}, originate from FORC measurements in $H = 0$ and from the irreversible component of the lower branch of the hysteresis loop, respectively. They are generated by **`CalculateFORC`** as part of the standard output. The third distribution, f_{cr}, is associated with the central ridge and is generated by **`IsolateCR`**. All three distributions are plotted by **`IsolateCR`** as seen in this example. f_{ir} is the only distribution that exists for positive and negative fields, like the hysteresis loop from which it is derived. Negative arguments of f_{ir} originate from irreversible magnetization processes that occur without reversing the field direction. Only non-interacting, uniaxial single-domain particles produce a strictly positive f_{ir}. **(e)** Total magnetizations derived from FORC measurements (M_s and M_{rs}), integration of the FORC diagram (M_{FORC}), and integration of the coercivity distributions shown in (d) (M_{bk}, M_{ir}, and M_{cr}).

Literature

Abrajevitch, A., K. Kodama (2011). Diagenetic sensitivity of paleoenvironmental proxies: A rock magnetic study of Australian continental margin sediments, *Geochemistry, Geophysics, Geosystems 12*, Q05Z24, doi:101029/2010GC003481.

Dunlop, D.J. (2002). Theory and application of the Day plot (M_{rs}/M_s versus H_{cr}/H_c) 2. Application to data for rocks, sediments, and soils, *Journal of Geophysical Research 107*, 2057, doi:10.1029/2001JB000487.

Egli, R. (2004). Characterization of individual rock magnetic components by analysis of remanence curves, 1. Unmixing natural sediments, *Studia Geophysica et Geodaetica 48*, 391-446.

Egli, R., A.P. Chen, M. Winklhofer, K.P. Kodama, C.S. Horng (2010). Detection of noninteractinig single domain particles using first-order reversal curve diagrams, *Geochemistry, Geophysics, Geosystems 11*, Q01Z11, doi:101029/2009GC002916.

Egli, R. (2013). VARIFORC: An optimized protocol for calculating non-regular first-order reversal curve (FORC) diagrams, *Global and Planetary Change 110*, 302-320, doi:10.1016/j.gloplacha.2013.08.003.

Fabian, K., T. von Dobeneck (1997). Isothermal magnetization of samples with stable Preisach function: A survey of hysteresis, remanence, and rock magnetic parameters, *Journal of Geophysical Research 102*, 17659-17677.

Fabian, K. (2006). Approach to saturation analysis of hysteresis measurements in rock magnetism and evidence for stress-dominated magnetic anisotropy in young mid-ocean ridge basalt, *Physics of the Earth and Planetary Interiors 154*, 299-307.

Friedrich, G., A.S. Schmitz-Wiechowski (1980). Mineralogy and chemistry of a ferromanganese crust from a deep-sea hill, Central Pacific, "Valdivia" Crusie VA13/2, *Marine Geology 37*, 71-90.

Gehring, A.U., J. Kind, M. Charilaou, I. García-Rubio (2011). The detection of magnetotactic bacteria and magnetofossils by means of magnetic anisotropy, *Earth and Planetary Science Letters 309*, 113-117.

Harrison, R.J., and J.M. Feinberg (2008). FORCinel: An improved algorithm for calculating first-order reversal curve distributions using locally weighted regression smoothing, *Geochemistry, Geophysics, Geosystems 9*, Q05016, doi:101029/2008GC001987.

Li, J., W. Wu, Q. Liu, and Y. Pan (2012). Magnetic anisotropy, magnetostatic interactions, and identification of magnetofossils, *Geochemistry, Geophysics, Geosystems 13*, Q10Z51, doi:101029/2012GC004384.

Lin, W., Y. Pan (2009). Uncultivated magnetotactic cocci from Yuandadu Park in Beijing, China, *Applied and Environmental Microbiology 75*, 4046-4052.

Muxworthy, A., W. Williams, D. Virdee (2003). Effect of magnetostatic interactions on the hysteresis parameters of single-domain and pseudo-single-domain grains, *Journal of Geophysical Research 108*, doi:10.1029/2003JB002588.

Newell, A.J. (2005). A high-precision model of first-order reversal curve (FORC) functions for single-domain ferromagnets with uniaxial anisotropy, *Geochemistry, Geophysics, Geosystems 6*, Q05010, doi:101029/2004GC000877.

Pan, Y., N. Petersen, M. Winklhofer, A.F. Davila, Q. Liu, T. Frederichs, M. Hanzlik, R. Zhu (2005). Rock magnetic properties of uncultured magnetotactic bacteria, *Earth and Planetary Sciences 237*, 311-325.

Pike, C.R., A.P. Roberts, K.L. Verosub (1999). Characterizing interactions in fine magnetic particle systems using first order reversal curves, *Journal of Applied Physics 85*, 6660-6667.

Pike, C.R., A.P. Roberts, K.L. Verosub (2001). First-order reversal curve diagrams and thermal relaxation effects in magnetic particles, *Geophysical Journal International 145*, 721-730.

Pike, C.R. (2003). First-order reversal-curve diagrams and reversible magnetization, *Physical Review B 68*, 104424.

Roberts, A.P., L. Chang, D. Heslop, F. Florindo, J.C. Larrasoaña (2012). Searching for single domain magnetite in the "pseudo-single-domain" sedimentary haystack: Implications of biogenic magnetite preservation for sediment magnetism and relative paleointensity determination, *Journal of Geophysical Research 117*, B08104, doi:10.1029/2012JB009412.

Winklhofer, M., G.T. Zimanyi (2006). Extracting the intrinsic switching field distribution in perpendicular media: A comparative analysis, *Journal of Applied Physics 99*, 08E710.